

# Collisionless energy absorption in the short-pulse intense laser-cluster interaction

M. Kundu and D. Bauer

Max-Planck-Institut für Kernphysik, Postfach 103980, 69029 Heidelberg, Germany

(Dated: July 8, 2021)

In a previous Letter [Phys. Rev. Lett. **96**, 123401 (2006)] we have shown by means of three-dimensional particle-in-cell simulations and a simple rigid-sphere model that nonlinear resonance absorption is the dominant collisionless absorption mechanism in the intense, short-pulse laser cluster interaction. In this paper we present a more detailed account of the matter. In particular we show that the absorption efficiency is almost independent of the laser polarization. In the rigid-sphere model, the absorbed energy increases by many orders of magnitude at a certain threshold laser intensity. The particle-in-cell results display maximum fractional absorption around the same intensity. We calculate the threshold intensity and show that it is underestimated by the common over-barrier ionization estimate.

PACS numbers: 36.40.Gk, 52.25.Os, 52.50.Jm

## I. INTRODUCTION

Intense laser-matter interaction provides a route to create energetic particles (e.g., electrons, ions, and photons) using table-top equipment. Clusters, possessing the transparency of gas targets and the high charge density of solid targets, proved to be very efficient absorbers of laser light. Their small size, compared to laser wavelength and skin depth, avoids reflection of the laser beam at the cluster surface as well as the loss of hot electrons into the cold bulk. In fact, almost 100% absorption of the laser light was reported in experiments with rare gas clusters [1]. Useful reviews on the subject are Refs. [2, 3, 4].

Upon irradiation of the rare gas clusters by intense laser light, electrons first absorb energy and leave their “parent” ions. This is known as inner ionization, meaning that the electrons are still bound to the cluster but not necessarily to their “parent” ions. The total electric field (i.e., laser plus space charge field) inside the cluster leads to inner ionization up to high charge states not possible with the laser field alone (ionization ignition [5, 6]). As the laser intensity during the pulse increases, these electrons absorb energy from the laser field and may leave the cluster leading to the positive charging of the cluster known as outer ionization. Thus outer ionization leads to a non-neutral plasma. With the increasing outer ionization, the restoring force of the ions counteracts ionization ignition so that the latter stops at some point. The net positive charge left behind finally explodes due to the Coulomb repulsion and hydrodynamic pressure, leading to the conversion of electron energy into ion energy. Typically MeV ions and keV electrons [7, 8, 9] are measured in experiments.

It is clear from the described scenario that the understanding of the relevant mechanism(s) of laser energy absorption leading to the heating of cluster electrons and outer ionization is of great importance for the development of a complete theoretical description.

Laser energy absorption by electrons proceeds either through resonances (linear or nonlinear) or through non-adiabaticities (all possible types of collisions). All of

these processes lead to dephasing of the current density with respect to the laser field, which, according to Poynting’s theorem, is a prerequisite for absorption. Collisional absorption via collisions of electrons with ions are of minor importance at near infrared wavelengths  $\simeq 800$  nm or greater [10, 11, 12, 13] whereas it is the dominant absorption mechanism at short wavelengths [13, 14, 15], not studied in this paper. The finite size of the clusters suggests that “collisions with the cluster boundary” may be responsible for the energy absorption. However, this viewpoint is misleading, as will be shown in Sec. II B.

During the expansion of the ionic core, the decreasing charge density  $\rho(t)$  leads to the decrease of the Mie plasma frequency,  $\omega_{\text{Mie}}(t) \equiv \sqrt{4\pi\rho(t)/3}$  (atomic units  $\hbar = m = -e = 4\pi\epsilon_0 = 1$  are used unless noted otherwise). For very short near infrared laser pulses  $\omega_{\text{Mie}}(t)$  cannot meet the linear resonance

$$\omega_{\text{Mie}}(t) = \omega_1, \quad (1)$$

unless the cluster has sufficiently expanded (typically after a few hundred femtoseconds). Linear resonance (1), well understood in theory, experiments, and simulations [16, 17, 18, 19, 20, 21, 22, 23, 24], is thus ruled out for very short pulses or during the early cycles of a long pulse laser-cluster interaction where ion motion is negligible. In this case, nonlinear resonance (NLR), whose origin lies in the anharmonicity of the cluster potential, turns out to be the dominant collisionless absorption mechanism. In fact, for very short linearly polarized (LP) laser pulses, it was clearly shown [25] that essentially *all* electrons that contribute to outer ionization pass through the NLR, which was unequivocally identified as *the* collisionless absorption mechanism in the absence of linear resonance. The eigenfrequency  $\omega[\hat{r}(t)]$  of a (laser-) driven oscillator in an anharmonic potential, being dependent on its excursion amplitude  $\hat{r}(t)$  (or the energy), may dynamically meet the NLR

$$\omega[\hat{r}(t)] = \omega_1. \quad (2)$$

Due to the many body nature of the interaction, the identification, the separation, and the interpretation of

the absorption mechanisms in molecular dynamics or particle-in-cell (PIC) simulations are often difficult. Recently, a method of identification of the NLR in many-body simulations of rare gas clusters has been proposed [25]. The possible importance of NLR was also mentioned or discussed previously [26, 27, 28, 29]. The rigid sphere model (RSM) [27, 30, 31] where electrons and ions are modeled by homogeneously charged rigid spheres oscillating against each other is clearly an oversimplification of a real many-particle system such as a cluster. However, it proves useful for estimating the order of magnitude of the absorbed energy as well as for the calculation of the laser intensity where energy absorption is most efficient, as will be shown in the present work. Moreover, it provides physical understanding and clearly displays NLR [25, 27].

The heating of cluster electrons in circularly polarized laser fields has not yet received much attention, at least theoretically. Experiments with rare-gas clusters show almost no effect on the x-ray emission [32, 33, 34] and ion energy distribution [35] when laser light of different ellipticity is used. Theoretically, circular polarization is particularly interesting because the above mentioned “collisions with the cluster boundary” are strongly suppressed in this case. Hence one may expect energy absorption being less efficient. NLR, on the other hand, occurs in both cases, and, in fact, the energy absorption turns out to be equally efficient. Moreover, the absorbed energy compares well with the RSM predictions.

The outline of the present paper is as follows: in Sec. II A we briefly review the NLR and the RSM. In Sec. II B the RSM is extended to circular polarization, where NLR is observed as well. In Sec. II C the RSM threshold intensities are calculated. Section III is devoted to the PIC [36] results for both linear and circular polarization. Finally, we summarize our results in Sec. IV.

Throughout this paper we use  $n = 8$ -cycle laser pulses of near infrared wavelength  $\lambda = 1056$  nm and a fixed cluster radius  $R = 3.2$  nm unless stated otherwise. NLR is a robust phenomenon that—qualitatively—is insensitive to cluster and laser parameters.

## II. NONLINEAR RESONANCE IN THE RIGID SPHERE MODEL (RSM)

The ion motion can be neglected in the study of energy absorption in very short laser pulses. Thus the ions just form a static, positively charged background of spherical shape. For not too high laser intensity, the collective motion of the electrons can also be approximated by a homogeneous, rigid sphere of negative charge. In the simplest case the radii of ion and electron sphere are assumed to be equal. In a more realistic model the electron cloud expands [27]. However, the method of identification of the NLR used in this paper is independent of the degree of electronic expansion. The center of mass of the electron-ion system is, in good approximation, located

at the center of the ion sphere. In an oscillating laser field, the homogeneously charged electron sphere oscillates back and forth against the positively charged ion sphere.

### A. NLR in a linearly polarized laser field

The equation of motion of the electron center of mass in a LP laser field, polarized along  $x$ , can be written as

$$\frac{d^2\bar{r}}{d\tau^2} + \frac{\bar{r}}{r}g(r) = -\frac{E_l(\tau)}{R\omega_l^2}, \quad (3)$$

where  $\bar{r} = x/R$  is the excursion of the electron sphere, normalized to the cluster radius  $R$ ,  $r = |\bar{r}|$ ,  $\tau = \omega_l t$  is the normalized time in units of the laser period, and the dimensionless electrostatic restoring force  $g(r)$  is

$$g(r) = \left(\frac{\omega_{\text{Mie}}}{\omega_l}\right)^2 \times \begin{cases} r - \frac{9r^2}{16} + \frac{r^4}{32} & 0 \leq r \leq 2 \\ \frac{1}{r^2} & r \geq 2 \end{cases}. \quad (4)$$

The first term in the upper line of (4) is the linear force when the displacement of the electron sphere is small, the next two terms are the nonlinear terms which appear due to the partial overlap of the electron cloud with the ion cloud. The term  $r^{-2}$  in the lower line of (4) is the Coulomb force between the separated electron sphere and ion sphere. The quantity on the right hand side of (3) is the normalized driver strength, which is the quiver amplitude  $E_l(\tau)/\omega_l^2$  of a free electron in the laser field  $E_l(\tau)$  normalized to the cluster radius  $R$ . Earlier work [27] showed that absorption of laser energy in the RSM is characterized by a threshold driver strength below which absorption is negligible (harmonic regime) and above which absorption is almost constant. Figure 1 shows this threshold behavior for  $(\omega_{\text{Mie}}/\omega_l)^2 = 10/3$  and a  $n = 8$ -cycle  $\sin^2$ -pulse  $E_l(\tau) = E_0 \sin^2(\tau/2n) \cos(\tau)$  for  $0 < \tau < 2n\pi$ . The dashed line is the absorption corresponding to a driven, purely harmonic oscillator

$$\frac{d^2\bar{r}}{d\tau^2} + \left(\frac{\omega_{\text{Mie}}}{\omega_l}\right)^2 \bar{r} = -\frac{E_l(\tau)}{R\omega_l^2} \quad (5)$$

in the laser field  $E_l(\tau)$ . The laser energy absorbed by a single electron in a  $n$ -cycle laser pulse of period  $T$  is

$$\frac{E_{\text{tot}}}{N} = - \int_0^{nT} \mathbf{v}(t) \cdot \mathbf{E}_l(t) dt. \quad (6)$$

Solving (5) analytically for the velocity  $v(t)$  and integrating (6) one finds for the absorbed energy per electron [27]

$$\frac{E_{\text{tot}}}{N} \simeq \frac{\omega_l^4 \omega_{\text{Mie}}^2 (\omega_{\text{Mie}}^2 + 3\omega_l^2)^2}{4n^4 (\omega_{\text{Mie}}^2 - \omega_l^2)^6} [1 - \cos(\omega_{\text{Mie}} n T)] E_0^2 \quad (7)$$

where  $[\omega_{\text{Mie}}^2 - (1 + 1/n)^2 \omega_l^2]^2 [\omega_{\text{Mie}}^2 - (1 - 1/n)^2 \omega_l^2]^2 \simeq (\omega_{\text{Mie}}^2 - \omega_l^2)^4$  (for sufficiently large  $n$ ) was used. The analytical estimate (7) is plotted in Fig. 1 together with the

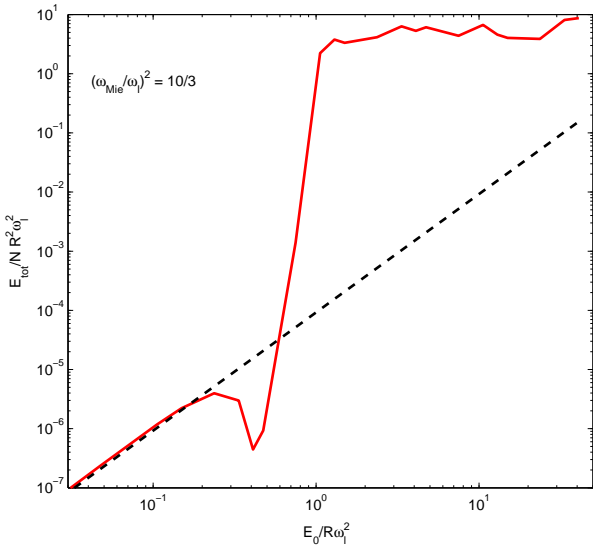


FIG. 1: (color online). Laser energy absorption vs driver amplitude in the rigid sphere-model for  $(\omega_{\text{Mie}}/\omega_l)^2 = 10/3$ , a  $n = 8$  cycle laser field  $E_l(\tau) = E_0 \sin^2(\tau/2n) \cos(\tau)$ , and cluster radius  $R = 3.2$  nm. Within a narrow field strength interval (here  $\simeq 0.5$ –1) the absorbed energy per particle (solid line) increases by many orders of magnitude. The dashed line represents the absorbed energy (7) by a purely harmonic oscillator driven by the same laser field.

absorbed energy obtained from the numerical solution of (3). One sees that the absorbed energy jumps by many orders of magnitude to a higher value after crossing a threshold driver strength. The higher the cluster charge density is, the higher is this threshold driver strength. The rigid sphere model shows this behavior of efficient absorption above the threshold driver strength at all cluster charge densities independent of the linear resonance condition  $\rho = 3\rho_c$ , contrary to the nanoplasma model [16]. Since the rigid sphere model does not necessarily requires expansion of the cluster for the efficient absorption of laser energy, it permits us to understand the behavior of energy absorption and the underlying mechanism for very short laser pulses.

Equation (3) can be formally rewritten as

$$\frac{d^2\bar{r}}{d\tau^2} + \left[ \frac{\omega_{\text{eff}}[\dot{r}(\tau)]}{\omega_l} \right]^2 \bar{r} = -\frac{E_l(\tau)}{R\omega_l^2}. \quad (8)$$

Equation (8) yields the instantaneous, scaled effective frequency squared

$$\left[ \frac{\omega_{\text{eff}}(\tau)}{\omega_l} \right]^2 = \frac{-\frac{E_l(\tau)}{R\omega_l^2} - \ddot{r}(\tau)}{\bar{r}(\tau)} = \frac{g[r(\tau)]}{r(\tau)} \quad (9)$$

which passes through unity at the NLR (2). The right hand side of (9) is the restoring force divided by the excursion of the electronic cloud, which in the case of harmonic motion would be the square of the characteristic

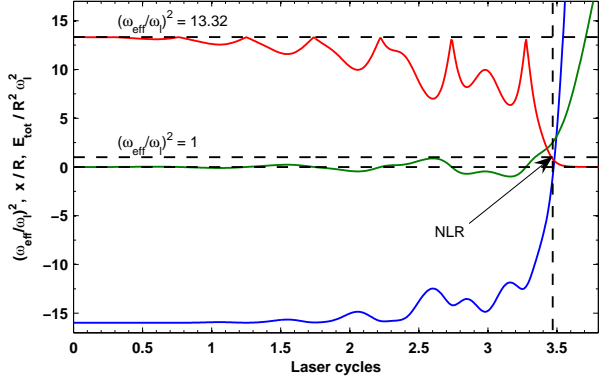


FIG. 2: (color online). Typical behavior of  $(\omega_{\text{eff}}(\tau)/\omega_l)^2$  (red, upper solid line) vs laser cycles above the threshold driver strength for  $(\omega_{\text{Mie}}/\omega_l)^2 = 40/3$ . Here we take  $E_0/R\omega_l^2 \simeq 7.48$  corresponding to a laser intensity  $\simeq 2.5 \times 10^{16} \text{ W/cm}^2$ , a  $n = 8$ -cycle  $\sin^2$ -pulse  $E_l(\tau) = E_0 \sin^2(\tau/2n) \cos(\tau)$  of wavelength  $\lambda = 1056$  nm, and a cluster radius  $R = 3.2$  nm. Excursion  $x/R$  (green, middle solid line) and energy of the electron sphere  $E_{\text{tot}}/R^2\omega_l^2$  (blue, lower solid line) are included in the plot. Outer ionization (i.e.,  $E_{\text{tot}}/R^2\omega_l^2 \geq 0$ ) and occurrence of NLR  $[\omega_{\text{eff}}(\tau)/\omega_l]^2 = 1$  always coincide (dashed vertical line).

frequency. Figure 2 shows a typical example of the temporal behavior of  $[\omega_{\text{eff}}(\tau)/\omega_l]^2$  above the threshold driver strength for  $(\omega_{\text{Mie}}/\omega_l)^2 = 40/3$ . Since  $(\omega_{\text{Mie}}/\omega_l)^2 = 13.32$ ,  $[\omega_{\text{eff}}(\tau)/\omega_l]^2$  starts at this value and drops with increasing driver strength. It passes through unity at the time indicated by the vertical line, and it is exactly at that time where the electron sphere becomes free (outer ionization). This incidence is clearly visible from the energy of the electron sphere, which passes through zero and the excursion as well. Outer ionization and occurrence of NLR happens for all driver strengths above the threshold whereas the resonance is never met below the threshold. Since the amplitude of the excursion of the electronic sphere depends upon the driver strength, the excursion amplitude should also be large enough so that the NLR is passed. The decrease in the effective frequency with the increase of the amplitude of excursion of the electronic sphere in the force field (3) can be understood by analyzing its motion in the corresponding anharmonic potential

$$V(r) = \omega_{\text{Mie}}^2 R^2 \times \begin{cases} \frac{r^2}{5} - \frac{3r^3}{16} + \frac{r^5}{160} & 0 \leq r \leq 2 \\ \frac{1}{r} & r \geq 2. \end{cases} \quad (10)$$

The period  $T$  of oscillation of the electronic sphere in the potential  $V(r)$  can be approximated by a perturbation series [37] as

$$T = \frac{1}{\sqrt{2}} \sum_{k=0}^{\infty} \frac{(-1)^k}{k!} \frac{\partial^k}{\partial E_{\text{tot}}^k} \oint \frac{[\delta V(r)]^k dr}{\sqrt{E_{\text{tot}} - V_0(r)}}. \quad (11)$$

Here,  $E_{\text{tot}}$  is the total energy of the electronic sphere in the ionic field,  $V_0(r) = \omega_{\text{Mie}}^2 R^2 r^2/2$  is the harmonic

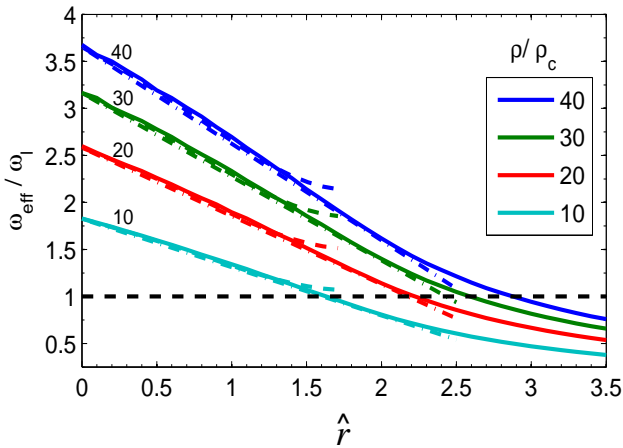


FIG. 3: (color online). Effective frequency  $\omega_{\text{eff}}/\omega_l$  vs the excursion amplitude  $\hat{r}$  of the electronic sphere for different cluster charge densities  $\rho/\rho_c = 10-40$ . The solid lines are computed from the numerical solution of (3). The dashed lines are the corresponding analytical approximations from (11) for  $k$  up to 6, and the dashed-dotted lines are from (12). For the charge density  $\rho/\rho_c = 40$  one expects NLR (horizontal dashed line) to occur at the excursion  $\hat{r} \simeq 2.88$ .

oscillator potential and  $\delta V(r) = \alpha R^3 r^3/3 + \beta R^5 r^5/5$  is the perturbation to the potential with  $\alpha = -9\omega_{\text{Mie}}^2/16R$  and  $\beta = \omega_{\text{Mie}}^2/32R^3$ . The effective frequency is then  $\omega_{\text{eff}} = 2\pi/T$ . For the excursion  $r < 2$  and cluster radius  $R = 3.2$  nm ( $\simeq 60.4$  a.u.) we can consider  $|\beta/\alpha| \ll 1$  and the approximate potential  $\delta V(r) \simeq \alpha R^3 r^3/3$ . Corrections up to  $k = 6$  yield  $T = T_0 + T_1 + \dots + T_6$ . The unperturbed period is  $T_0 = 2\pi/\omega_{\text{Mie}}$  and the successive corrections are  $T_1 = c_1/(3\omega_{\text{Mie}}^4)$ ,  $T_2 = c_2/(3\omega_{\text{Mie}}^7)$ ,  $T_3 = c_3/(9\omega_{\text{Mie}}^{10})$ ,  $T_4 = c_4/(72\omega_{\text{Mie}}^{13})$ ,  $T_5 = c_5/(54\omega_{\text{Mie}}^{16})$ ,  $T_6 = c_6/(36\omega_{\text{Mie}}^{19})$  with  $c_1 \simeq -8\alpha(2E_{\text{tot}})^{1/2}$ ,  $c_2 \simeq 5\pi\alpha^2 E_{\text{tot}}$ ,  $c_3 \simeq -28.45\alpha^3(2E_{\text{tot}})^{3/2}$ ,  $c_4 \simeq 385\pi\alpha^4 E_{\text{tot}}^2$ ,  $c_5 \simeq -318.6\alpha^5(2E_{\text{tot}})^{5/2}$  and  $c_6 \simeq 97.89 \times 2^9 \alpha^6 E_{\text{tot}}^3$ , respectively.

Neglecting the higher order term of  $g(r)$  for  $r < 2$ , a simpler approximation to the effective frequency can be derived from (9) by replacing the excursion  $r$  with the excursion amplitude  $\hat{r}$ :

$$\omega_{\text{eff}}(\hat{r}) \simeq \omega_{\text{Mie}} (1 - 9\hat{r}/16)^{1/2} \simeq \omega_{\text{Mie}} (1 - 9\hat{r}/32). \quad (12)$$

Figure 3 shows the effective frequency vs the excursion amplitude  $\hat{r}$  of the electronic sphere in the potential (10) for various cluster charge densities  $\rho/\rho_c = 10-40$  as calculated from the numerical solution of (3) together with the approximations (11) and (12). The effective frequency as calculated from (11) shows good agreement below the excursion  $\hat{r} < 1.5$  and low charge densities (e.g.,  $\rho/\rho_c < 10$ ). For higher charge densities more corrections [large number of  $k$  values in (11)] are needed, which are very much cumbersome to calculate. Although (12) fits well with the numerical solution,  $\omega_{\text{eff}}$  becomes negative when  $\hat{r} > 32/9$ . However, the results using (12) agree with the exact ones

in Fig. 3 up to  $\rho/\rho_c = 30$  for the excursions of interest, i.e., up to the point where the electronic sphere undergoes NLR. The variation of frequency with the excursion amplitude as shown in Fig. 3 explains why a threshold driver strength is required for an appreciable laser energy absorption as well as for the crossing of the NLR in the Fig. 2: only a driver exceeding a certain threshold field strength will lead to excursions compatible with the NLR condition  $\omega_{\text{eff}} = \omega_l$ .

## B. NLR in a circularly polarized laser field

Clusters in a circularly polarized (CP) laser field received less attention in the literature. It is not known *a priori* how the outer ionization and energy absorption by clusters depend on the laser polarization. In laser-atom interaction the laser polarization has dramatic effects: since in CP the free electrons do not return to their parent atom all the atomic effects relying on rescattering such as high-order harmonic generation, high-order above-threshold ionization, and nonsequential ionization are strongly suppressed. In the context of clusters, the study of the absorption efficiency as a function of the laser polarization can help to discriminate among different absorption mechanisms. For instance, if laser energy absorption was indeed due to “collisions with the cluster boundary” it would be suppressed in CP because the electrons mainly swirl around parallel to the “cluster boundary” rather than crossing (and hence colliding) with it. However, as we will show, the absorption of laser energy is largely independent of the laser polarization, thus ruling out “collisions with the cluster boundary” as a meaningful absorption mechanism.

### 1. Two-dimensional rigid sphere model

Let us first extend the RSM to CP. In a CP laser field with electric field components in  $x$ - and  $y$ -direction, the equation of motion for the electronic sphere in the rigid sphere approximation of a cluster can be written as

$$\left\{ \begin{array}{l} \ddot{r}_x \\ \ddot{r}_y \end{array} \right\} + \frac{g(r)}{r} \left\{ \begin{array}{l} r_x \\ r_y \end{array} \right\} = -\frac{1}{R\omega_l^2} \left\{ \begin{array}{l} E_l^x(\tau) \\ E_l^y(\tau) \end{array} \right\}. \quad (13)$$

Here,  $r_x = x/R$ ,  $r_y = y/R$ ,  $r = \sqrt{r_x^2 + r_y^2}$ , and

$$E_l^x(\tau) = \frac{E_0}{\sqrt{2}} \sin^2(\tau/2n) \cos(\tau), \quad (14)$$

$$E_l^y(\tau) = \frac{E_0}{\sqrt{2}} \sin^2(\tau/2n) \sin(\tau). \quad (15)$$

One identifies  $E_x = g(r)r_x/r$  and  $E_y = g(r)r_y/r$  as the two components of the restoring force in (13). Note that we have divided the electric field components by a factor  $\sqrt{2}$  so that the ponderomotive energy  $U_p = E_0^2/4\omega_l^2$ , (i.e., the time-averaged quiver energy of a free electron in the

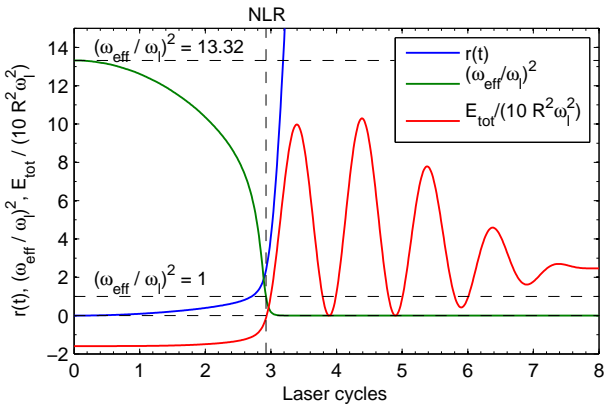


FIG. 4: (color online). Typical behavior of  $(\omega_{\text{eff}}(\tau)/\omega_l)^2$  (green, top left solid line) vs laser cycles above the threshold driver strength  $\simeq 3 \times 10^{16} \text{W/cm}^2$  for circular polarization,  $(\omega_{\text{Mie}}/\omega_l)^2 = 40/3$ , and cluster radius  $R = 3.2 \text{ nm}$ . Here,  $E_0/R\omega_l^2 \simeq 8.2$ , corresponding to a laser intensity  $\simeq 5 \times 10^{16} \text{W/cm}^2$ ,  $n = 8-cycle  $\sin^2$ -pulse with components  $E_l^x(\tau) = E_0 \sin^2(\tau/2n) \cos(\tau)/\sqrt{2}$ ,  $E_l^y(\tau) = E_0 \sin^2(\tau/2n) \sin(\tau)/\sqrt{2}$ , and wavelength  $\lambda = 1056 \text{ nm}$ . Excursion  $r$  (blue, middle left solid line) and energy  $E_{\text{tot}}/R^2\omega_l^2$  (red, bottom left solid line) are also plotted. The energy  $E_{\text{tot}}/R^2\omega_l^2$  is scaled down by a factor 10 to display within the excursion and the frequency range. Outer ionization (i.e.,  $E_{\text{tot}}/R^2\omega_l^2 \geq 0$ ) and occurrence of NLR  $[\omega_{\text{eff}}(\tau)/\omega_l]^2 = 1$  always coincide (dashed vertical).$

laser field) is the same as in the LP case with the same  $E_0$  (otherwise  $U_p$  would be a factor of two higher in the CP case). The square of the effective, time-dependent oscillator frequency in the CP laser field can be written as

$$\left[ \frac{\omega_{\text{eff}}(\tau)}{\omega_l} \right]^2 = \frac{r_x E_x + r_y E_x}{r^2} = \frac{g[r(\tau)]}{r(\tau)}, \quad (16)$$

which has the same form as in the LP case (9). Earlier, in Fig. 2, it was shown that NLR and outer ionization in the RSM only occur when a threshold laser intensity is crossed. The same is true for the occurrence of NLR with CP light. Figure 4 shows the temporal behavior of  $[\omega_{\text{eff}}(\tau)/\omega_l]^2$  above the threshold driver strength for a  $n = 8-cycle CP laser pulse of wavelength  $\lambda = 1056 \text{ nm}$ . Here the cluster charge density is 40 times over-critical, i.e.,  $(\omega_{\text{Mie}}/\omega_l)^2 = 13.32$  at which  $(\omega_{\text{eff}}(\tau)/\omega_l)^2$  starts and drops with increasing driver field during the pulse. The NLR  $[\omega_{\text{eff}}(\tau)/\omega_l]^2 = 1$  is passed at the time indicated by the vertical line. As in the LP case in Fig. 2, the electron sphere is set free at the time the NLR is passed: the energy of the electron sphere passes through zero, and the excursion sharply increases to a high value. It is also clear from Fig. 4, that once the electronic sphere is set free, the frequency drops to zero, and the total absorbed energy remains positive. A zero effective frequency implies an infinite period, i.e, the electron sphere does not return to the ion sphere. The main difference between Fig. 4 and Fig. 2 is that in the case of the CP laser field$

the decrease of the effective frequency is smooth (i.e., no oscillations) since the electric field vector rotates but its absolute value remains constant. As a consequence, the electron sphere spirals out, staying away from the potential center where  $\omega_{\text{eff}} = \omega_{\text{Mie}}$ . For LP instead, the electron sphere is driven through the origin and hence the effective frequency undergoes oscillations before it drops to the resonance value, as visible in Fig. 2. NLR is clearly identified in both cases.

### C. Prediction of threshold intensity for the NLR

NLR occurs above a threshold driver strength. Beyond this driver strength the rigid electron sphere gains laser energy which is many order of magnitude higher than below the threshold (see Fig. 1). In an open potential such as (10) the electron sphere is detached from the ion sphere above the threshold driver strength, i.e., appreciable energy absorption and outer ionization occur simultaneously. We would like to remark that in closed potentials NLR occurs as well, as discussed in Ref. [28].

The threshold driver strength can be estimated. The dimensionless potential  $U(r) = V(r)/(\omega_{\text{Mie}}^2 R^2)$  of the electron sphere in the ionic field can be written as

$$U(r) = \frac{r^2}{2} - \frac{3r^3}{16} + \frac{r^5}{160}, \quad r \leq 2. \quad (17)$$

Application of a static electric field  $E_0$  (corresponding to the peak field strength of a low-frequency laser field), suppresses the potential in one direction by the amount  $RE_0 r$ . The effective potential seen by the electron sphere is  $U_{\text{eff}}(r) = U(r) - \hat{E}_0 r$  with  $\hat{E}_0 = E_0/(\omega_{\text{Mie}}^2 R)$ . The potential barrier vanishes if  $U'(r_v) - \hat{E}_0 = 0$  and  $U''(r_v) = 0$ , leading to  $r_v = 1$ , and the NLR threshold intensity is estimated to be

$$I_{\text{th}}^{\text{VBA}} = E_0^2 = \left( \frac{5}{32} \frac{\rho}{\rho_c} \omega_l^2 R \right)^2. \quad (18)$$

We call this the vanishing-barrier-approximation (VBA).

In atomic ionization the so-called over-the-barrier approximation (OBA) or Bethe-rule [38] allows to estimate at which electric field strength a certain atomic charge state dominates. If one applies the OBA to the RSM one obtains the two equations  $U_{\text{eff}}(r_b) = 0$  and  $U'(r_b) - \hat{E}_0 = 0$  with  $r_b$  the barrier location. One finds  $r_b \simeq 1.613$ . This gives the OBA threshold intensity of the NLR

$$I_{\text{th}}^{\text{OBA}} \simeq \left( \frac{10}{83} \frac{\rho}{\rho_c} \omega_l^2 R \right)^2, \quad (19)$$

which underestimates the numerically determined threshold intensity, as we will show now.

Figure 5 shows the threshold intensity as a function of the cluster charge density  $\rho/\rho_c = 10\text{--}160$  (corresponding to average charge states  $\simeq 1\text{--}16$  for Xenon). The numerically determined threshold intensities for LP (3) and CP

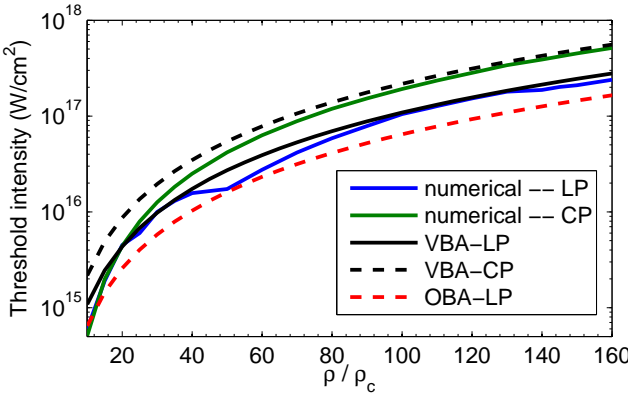


FIG. 5: NLR threshold intensities in the RSM vs the cluster charge density  $\rho/\rho_c$  for linearly (LP) and circularly (CP) polarized laser fields. Results from the full numerical solution of (3) with LP (lower solid), (13) CP (top solid), the vanishing barrier approximation (VBA-LP, middle solid) (18), and the VBA corrected for CP (upper dashed) are shown (see text for a discussion). The over-the-barrier approximation (OBA) (19) (lower dashed) underestimates the exact threshold intensities.

(13) laser light show that when the cluster charge density is low, the NLR occurs almost at the same value of the threshold intensity, irrespective of the polarization. As the charge density increases the NLR threshold intensity appears to be higher for CP than for LP. The VBA (18) of the threshold intensity is in good agreement with the numerical result for LP whereas the OBA (19) underestimates it. This fact might be related to the recently observed “enhanced saturation intensities” in the ionization of finite size systems such as  $C_{60}$  (see, e.g., [39, 40] and references therein), indicating that the latter might neither be a many-electron nor a quantum effect but just due to the finite size of the target.

The difference of the threshold intensities for LP and CP is due to the definition of the CP field (14), (15) where a factor  $2^{-1/2}$  has been introduced in order to render the ponderomotive potential equal for LP and CP. However, for the threshold intensity it is the electric field (or the intensity) that matters, not  $U_p$ . For a given  $E_0$  the laser intensity is  $I_0 = E_0^2$  in the LP case but only  $I_0/2$  for CP. Therefore, the upper black, dashed line in Fig. 5 shows the VBA threshold intensity multiplied by a factor of two, which is in good agreement with the numerical results for the CP laser field at higher charge densities.

So far we have studied the NLR absorption of laser energy in a simplified model system assuming an anharmonic potential generated by the ions in which the homogeneous and rigid electron cloud moves. In reality, the potential builds up during the interaction with the laser pulse because of ionization. The delicate interplay of inner ionization, energy absorption by various mechanisms, and outer ionization can be simulated using methods such as PIC or molecular dynamics. Previous work [25], studying LP short laser pulses, showed that NLR

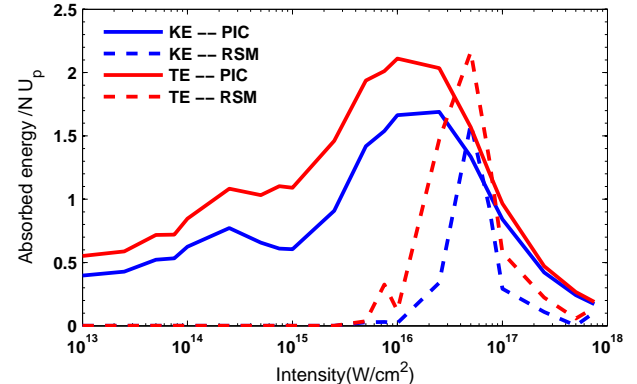


FIG. 6: (color online). Kinetic energy (KE) and total absorbed (TE) energy per electron in units of  $U_p$  vs laser intensity for charge density 40 times the critical density and a  $Xe_{1611}$  cluster ( $N = 5498$  electrons, mean ionic charge state  $\simeq 3.4$ , and a cluster radius  $R = 3.2$  nm). Solid lines are PIC results, dashed lines are the RSM results for a  $n = 8$  cycle pulse  $E_l(t) = E_0 \sin^2(\omega_l t/2n) \cos(\omega_l t)$  of wavelength  $\lambda = 1056$  nm.

(2) can be clearly identified in such simulations as well.

### III. NONLINEAR RESONANCE: PARTICLE-IN-CELL RESULTS

In this Section we present results obtained from three-dimensional PIC simulations. The cluster is exposed to  $n = 8$ -cycle  $\sin^2$ -pulses  $E_l(t) = E_0 \sin^2(\omega_l t/2n) \cos(\omega_l t)$  of near infrared wavelength  $\lambda = 1056$  nm, i.e., the total pulse duration is 28 fs. Since motion of ions does not play an important role during the entire pulse the ions are assumed fixed, which ensures a well defined, constant Mie frequency  $\omega_{\text{Mie}}$ . A PIC electron has the same charge to mass ratio as a “real” electron, that is,  $e/m = -1$  in atomic units. Each PIC electron moves under the influence of the external laser field and the space charge field  $\mathbf{E}_{\text{sc}} = -\nabla\Phi(\mathbf{r}, t)$  due to the potential  $\Phi(\mathbf{r}, t)$  that is created by all charges (mapped to the numerical grid). Hence the equation of motion of the  $i$ -th PIC electron is

$$\ddot{\mathbf{r}}_i + \mathbf{E}_{\text{sc}}(\mathbf{r}_i, t) = -\mathbf{E}_l(t). \quad (20)$$

Equation (20) is solved self-consistently for all PIC electrons. Clearly,  $\mathbf{E}_{\text{sc}}(\mathbf{r}_i, t)$  depends on the position of *all* other particles  $\neq i$  as well. The PIC simulation starts with the neutral cluster configuration so that  $\mathbf{E}_{\text{sc}}(\mathbf{r}_i, 0) \equiv 0$ .

#### A. Results for linear polarization

Figure 6 shows PIC results for the kinetic energy (KE) and the total energy (TE) absorbed per electron in units of  $U_p$ , vs the peak laser intensity. One sees that the

absorbed energy per electron is on the order of  $U_p$ . However, the absorbed energy is nonlinear in  $U_p$  and displays a maximum before it drops because of the saturation of outer ionization. The depletion is due to the fact that at a given intensity most (if not all) electrons are removed from the cluster (complete outer ionization). Further inner ionization would be required to generate “fresh” electrons that could continue to absorb energy. The maxima in the PIC absorption curves are located close to the threshold intensity predicted by the RSM. The total absorbed energy around the maximum of the PIC absorption curves (RSM as well) is on the order of  $2U_p = 5\text{--}6\text{ keV}$  which has been also reported in experiments of intense laser clusters interactions [8].

In PIC simulations no sharp intensity threshold exists since each PIC electron sees its own time-dependent field (space charge field plus the laser field). Therefore sharp jumps (as seen in the RSM, e.g., Fig. 1) are absent.

Figure 7 compares the kinetic and potential energies of a single PIC electron and the electronic sphere in the RSM. The energies are plotted vs the excursion  $x/R$  (along the direction of the laser field). The peak laser intensity is  $I_0 = 2.5 \times 10^{16} \text{ W/cm}^2$ . We have checked that there are many PIC electrons that leave the cluster similarly to the one presented in Fig. 7. The potential and the kinetic energy gained by the electron sphere in the RSM is divided by the total number of PIC electrons so that a quantitative comparison is possible. The main difference between PIC and RSM results is that in the PIC simulation all the electrons see initially a zero potential since the potential builds up from the neutral cluster configuration in the course of the interaction with the laser field while in the RSM the electronic sphere oscillates in a prescribed potential. Those PIC electrons that stay long inside the cluster experience almost the full ionic potential which then is similar to the RSM potential.

As mentioned earlier, the absorption of energy by a PIC electron depends upon the self-consistent potential which develops during the laser pulse due to outer ionization. As a result different PIC electrons move along different trajectories, “see” a different potential, and thus are set free at different times. Figure 8 shows a snapshot of the collective potential  $\Phi(\mathbf{r}, t)$  at time  $\omega_1 t / 2\pi = 4.81$  for a cut at  $z = 0$  (and various  $y$  throughout the cluster). The most lower curve represents the potential for  $y = z = 0$ . The red circles represent the total energy  $E_{\text{tot},i} = \dot{\mathbf{r}}_i^2(t)/2 - \Phi(\mathbf{r}_i, t)$  of individual PIC electrons located within the simulation box at that time.

One observes that many PIC electrons are accumulated near the bottom-left of the potential well at this time. These PIC electrons with  $E_{\text{tot},i} < 0$  remain bound since the laser field amplitude is already decreasing from the 4th cycle onward. The kinetic and the total energy of a PIC electron which leaves the potential well when its excursion becomes  $x/R \simeq 2.88$  at the same time is also shown. This excursion approximately satisfies the NLR condition  $\omega_{\text{eff}}/\omega_1 = 1$  for the charge density  $\rho/\rho_c = 40$ ,

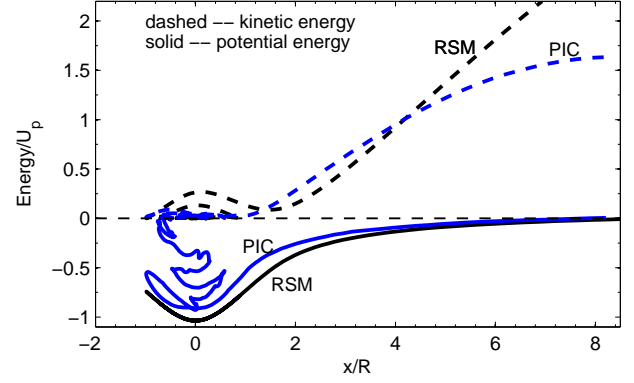


FIG. 7: (color online). Comparison between the kinetic and the potential energies of a PIC electron and the equivalent RSM electronic particle with same charge and mass of a PIC electron vs the excursion  $x/R$  in the laser polarization direction. The escaping PIC electron resembles the equivalent electronic particle in the RSM. Peak laser intensity  $I_0 = 2.5 \times 10^{16} \text{ W/cm}^2$ , charge density is  $\rho/\rho_c = 40$ . Other parameters as in Fig. 6.

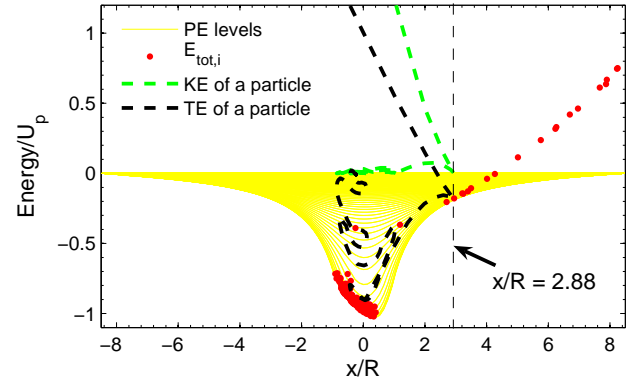


FIG. 8: (color online). Energy and self-consistent potential  $\Phi$  from the PIC simulation vs the excursion  $x/R$  in laser polarization direction. Yellow (solid gray) lines represent cuts of the potential  $\Phi$  at time  $\omega_1 t / 2\pi = 4.81$  for different  $y$  and  $z = 0$ . The circles (red) represent the total energy  $E_{\text{tot},i}$  of individual PIC electrons located within the simulation box at that time. The dashed lines represent the kinetic (green, dashed gray) energy (KE) and potential (dashed black) energy (PE) of a PIC electron that is outer ionized when the excursion  $x/R \simeq 2.88$  meets the condition  $\omega_{\text{eff}} = \omega_1$  at the same time (see Fig. 3 for the charge density  $\rho/\rho_c = 40$ ). The peak laser intensity is  $I_0 = 2.5 \times 10^{16} \text{ W/cm}^2$ . Other parameters as in Fig. 7.

as identified in Fig. 3 with the RSM analysis.

The NLR behavior exhibited by the PIC electron in Fig. 8 is not accidental. For the sake of an unequivocal and explicit identification of the NLR we now analyze the motion of all individual PIC electrons in the same way as it has been done with the motion of the electron sphere in the RSM in Sec. II. Recalling (20), the equation for the

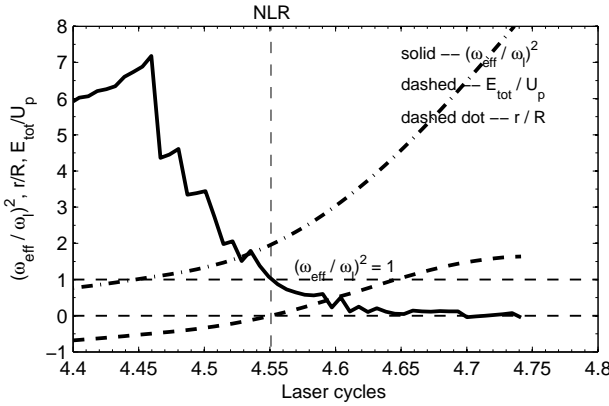


FIG. 9: Effective frequency squared  $(\omega_{\text{eff},i}/\omega_1)^2$ , excursion  $r_i/R$ , and the total energy  $E_{\text{tot},i} = \dot{r}_i^2(t)/2 - \Phi(\mathbf{r}_i, t)$  for the PIC electron of Fig. 7 vs time in laser cycles. The total energy becomes positive only when the NLR is crossed (indicated by the vertical dashed line). This result resembles the RSM result in Fig. 2 when NLR is met. The charge density is  $\rho/\rho_c = 40$ , the peak laser intensity is  $I_0 = 2.5 \times 10^{16} \text{ W/cm}^2$ . Other parameters as in Fig. 7.

effective, time-dependent oscillator frequency analogous to (16) for the  $i$ -th PIC electron reads

$$\omega_{\text{eff},i}^2(t) = -\frac{[\mathbf{E}_l(t) + \dot{\mathbf{r}}_i(t)] \cdot \mathbf{r}_i(t)}{\dot{\mathbf{r}}_i^2(t)} = \frac{\mathbf{E}_{\text{sc}}(\mathbf{r}_i, t) \cdot \mathbf{r}_i(t)}{\dot{\mathbf{r}}_i^2(t)}. \quad (21)$$

Earlier we have mentioned that  $\mathbf{E}_{\text{sc}}(\mathbf{r}_i, t)$  depends on the position of *all* other particles  $\neq i$  and the simulation starts with the charge neutral cluster configuration i.e.,  $\mathbf{E}_{\text{sc}}(\mathbf{r}_i, 0) \equiv \mathbf{0}$ . Hence, a PIC electron “sees” initially an effective frequency  $\omega_{\text{eff},i}(0) = 0$ . The laser field disturbs the charge equilibrium and  $\omega_{\text{eff},i}^2(t)$  becomes different from zero.  $\omega_{\text{eff},i}^2(t)$  may be even negative in regions of accumulated electron density (repulsive potential). As the cluster charges up,  $(\omega_{\text{eff}}/\omega_1)^2$  quickly increases beyond unity (where the RSM starts in the first place). The start from  $\omega_{\text{eff},i}(0) = 0$ , the possibility of negative  $\omega_{\text{eff},i}^2(t)$ , and the three-dimensionality are the main differences to the RSM analysis above. Figure 9 shows the effective frequency squared, the total energy  $E_{\text{tot},i}(t)$ , and the excursion  $r_i/R$  vs time for the PIC electron whose energy history is shown in Fig. 7. We define the time when, for a particular electron,  $E_{\text{tot},i}$  becomes  $> 0$  as the ionization time of that electron. Data are plotted shortly before the emission of this particle from the cluster potential. It is clearly visible in Fig. 9 that the PIC electron is escaped only when the resonance line  $(\omega_{\text{eff}}/\omega_1)^2 = 1$  is passed. Figure 9 can be well compared with Fig. 2 showing ionization of the RSM via NLR.

In the case of PIC simulations the fulfillment of the nonlinear resonance condition  $(\omega_{\text{eff}}/\omega_1)^2 = 1$  is necessary but not sufficient for ionization. As the potential builds up, the PIC electrons transiently meet the NLR condition, and, in fact, some electrons leave the cluster at that early stage when the potential is still shallow and

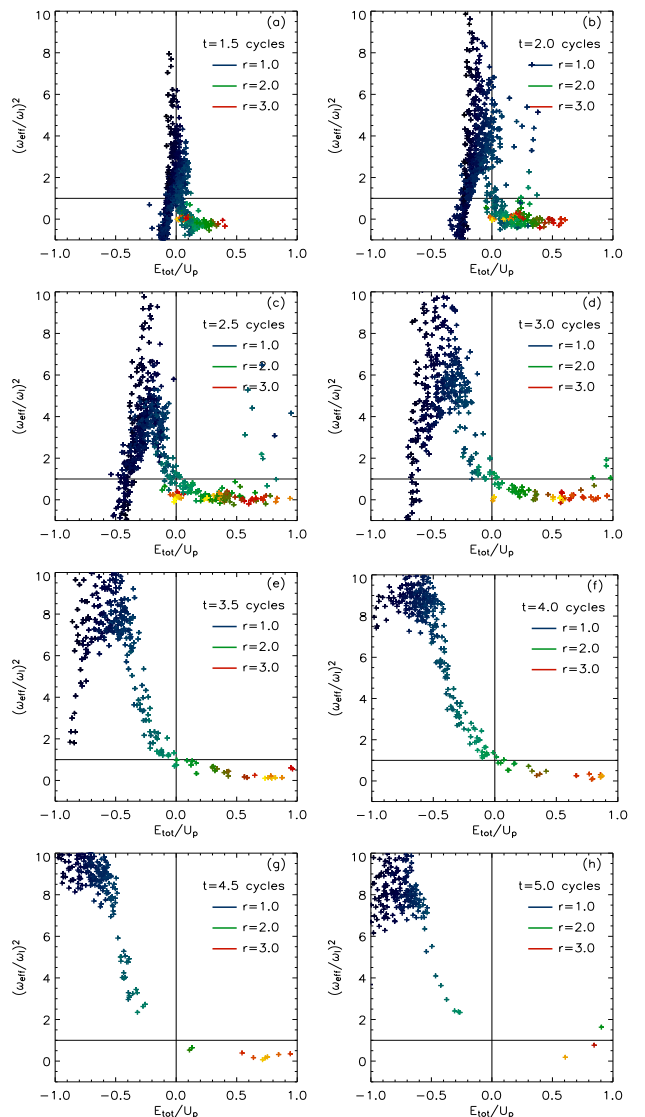


FIG. 10: (color online). Snapshots of PIC electrons in the frequency vs energy-plane at times (a)  $t = 1.5$ , (b)  $t = 2.0$ , (c)  $t = 2.5$ , (d)  $t = 3.0$ , (e)  $t = 3.5$ , (f)  $t = 4.0$ , (g)  $t = 4.5$ , and (h)  $t = 5.0$  laser cycles for LP, laser intensity  $2.5 \times 10^{16} \text{ Wcm}^{-2}$ , and  $(\omega_{\text{Mie}}/\omega_1)^2 = 40/3$ . Other parameters as in Fig. 9. The radial positions (in units of  $R$ ) are color-coded. Electrons become free upon crossing the NLR, i.e.,  $(\omega_{\text{eff}}^2/\omega_1^2, E_{\text{tot}}/U_p) = (1, 0)$ .

the laser field is relatively weak. However, as the potential deepens, PIC electrons “dropping” below the energy necessary for NLR to occur, behave from then on similar to the RSM and may finally escape only by climbing up in the potential and hitting the NLR  $(\omega_{\text{eff}}/\omega_1)^2 = 1$ . During the 0.4 laser cycles plotted in Fig. 9 the  $(\omega_{\text{eff}}/\omega_1)^2$ -curve displays artificial, short-time scale fluctuations inherent in PIC simulations [36]. However, we checked that macroscopic observables such as the absorbed energy or the degree of outer ionization are well converged.

By following the dynamics of the electrons in the ef-

fective frequency vs energy-plane we identify the main pathway to outer ionization and efficient absorption. Figure 10a–h shows the scaled effective frequencies squared  $(\omega_{\text{eff}}/\omega_l)^2$  of the individual PIC electrons vs their energies  $E_{\text{tot}}(t) = \dot{r}_i^2(t)/2 - \Phi(\mathbf{r}_i, t)$  they would have if the driver is switched off instantaneously at  $t = 1.5, 2, 2.5, 3, 3.5, 4, 4.5$ , and 5 laser cycles, respectively. At the time when, for a particular electron,  $E_{\text{tot}}$  becomes  $> 0$  the ionization occurs for that electron. The laser intensity is  $2.5 \times 10^{16} \text{ W cm}^{-2}$ , and the pre-ionized cluster is 40 times over-critical so that  $(\omega_{\text{Mie}}/\omega_l)^2 = 40/3$ . As is clearly visible in Fig. 10, each electron reaches positive energy close to the point  $(\omega_{\text{eff}}^2/\omega_l^2, E_{\text{tot}}/U_p) = (1, 0)$ . The radial position of each electron is color-coded, indicating that outer ionization occurs at radii around  $2R$ . During the early time of the laser pulse (Fig. 10a,b) when many electrons are still inside the cluster,  $(\omega_{\text{eff}}/\omega_l)^2$  spreads over a wide range, starting from the maximum value  $(\omega_{\text{Mie}}/\omega_l)^2$  down to negative values due to the repulsive force exerted by the compressed electronic cloud. Note that negative values in effective frequency occur mainly at early times where most of the electrons are still inside the cluster. Electrons with positive but very small  $E_{\text{tot}}$  and  $\omega_{\text{eff}}^2 \simeq 0$  represent low energetic electrons removed earlier during the pulse (see Fig. 10a,b). The occurrence of NLR is less clear for these early leaving electrons. As mentioned above, these electrons move in a shallow effective potential with  $(\omega_{\text{eff}}/\omega_l)^2 < 1$  when they leave the cluster with ease and with rather low kinetic energy because the laser intensity is still low at the time of their emission. Figures 10c–f show that most of the electrons escape from the cluster by passing through the channel  $(\omega_{\text{eff}}^2/\omega_l^2, E_{\text{tot}}/U_p) = (1, 0)$  at radii around  $2R$ . It is also visible that more and more electrons are driven to positive frequency before they leave the cluster by passing through  $(\omega_{\text{eff}}^2/\omega_l^2, E_{\text{tot}}/U_p) = (1, 0)$ . This is so because as more and more electrons are freed, the remaining electrons experience predominantly the force by the ionic background, and they move deep into the potential (see their negative values in energy) where they experience the full Mie-frequency  $\omega_{\text{Mie}}/\omega_l = 40/3$ . In Fig. 10c,d, the few electrons with positive energy but small radii are those driven back to the cluster by the laser field. In Figures 10e,f, electrons are strongly aligned (no scattered points) since the laser field is approaching its maximum (at  $t = 4$ -cycles). After the peak of the laser pulse (Figs 10g,h) the restoring force of the ions on almost all electrons dominates the laser force.

## B. Results for circular polarization

Since many of the features of energy absorption and NLR in a LP laser field are common to the case of CP, we only point out the main differences. Equation (21) holds in the CP laser field as well. Figure 11 shows the effective frequency squared vs time for one of the PIC electrons, together with the total energy  $E_{\text{tot},i}(t)$  and

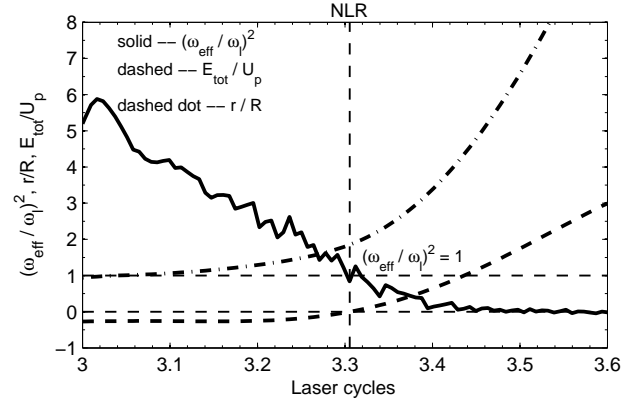


FIG. 11: Effective frequency squared  $(\omega_{\text{eff},i}/\omega_l)^2$ , excursion  $r_i/R$ , and the total energy  $E_{\text{tot},i} = \dot{r}_i^2(t)/2 - \Phi(\mathbf{r}_i, t)$  for a PIC electron in a CP field vs time in laser cycles. The total energy becomes positive only when the NLR is crossed (indicated by vertical, dashed line). This result resembles the RSM result in Fig. 4. The charge density is  $\rho/\rho_c = 40$ , the peak laser intensity is  $I_0 = 2.5 \times 10^{16} \text{ W/cm}^2$ .

the excursion  $r_i/R$ . One can see that the PIC electron is freed (i.e., its total energy becomes positive) only when the resonance line  $(\omega_{\text{eff}}/\omega_l)^2 = 1$  is passed.

Figure 12 is the CP analogue of Fig. 10. The results are very much similar to the LP case shown in Fig. 10 and the arguments made there apply here as well. NLR is clearly observed. The main difference is that the PIC electrons are nicer aligned towards the resonance point, even at early times during the laser pulse (see Fig. 12 b, c, d). Almost no scattered particles are visible because the dynamics mainly consist of swirling around the cluster center rather than oscillating through it. The number of electrons returning to the cluster is much less so that the recombination and rescattering probability is smaller in the case of CP. The same is observed in laser-atom interaction experiments, with important consequences for harmonic generation and non-sequential ionization.

For sufficiently high charge density, the degree of outer ionization (defined as the ratio of removed electrons to the total number of electrons) is less compared to the case of LP laser pulses. The explanation is the same as in Sec.IIC: the effective laser intensity for CP is by a factor of two lower than for LP because of our definition of the CP field (14), (15).

One may object that, since the denominator in (21) necessarily increases while the numerator decreases for an electron on its way out of the cluster potential, that the passage through a point  $(\omega_{\text{eff}}^2/\omega_l^2, E_{\text{tot}}/U_p) = (x, 0)$  with  $x$  some value  $< (\omega_{\text{Mie}}/\omega_l)^2$  is rather the consequence of outer ionization than the mechanism behind it. However, NLR only occurs at  $x = 1$ , and the results in Fig. 10 and Fig. 12 show only little spreading along  $(\omega_{\text{eff}}/\omega_l)^2$  at  $E_{\text{tot}} = 0$ . Moreover, the fact that *both* the single electron energies become positive *and* the radii exceed  $\simeq 2R$  when  $(\omega_{\text{eff}}/\omega_l)^2 = 1$  indicates that NLR is indeed the responsi-

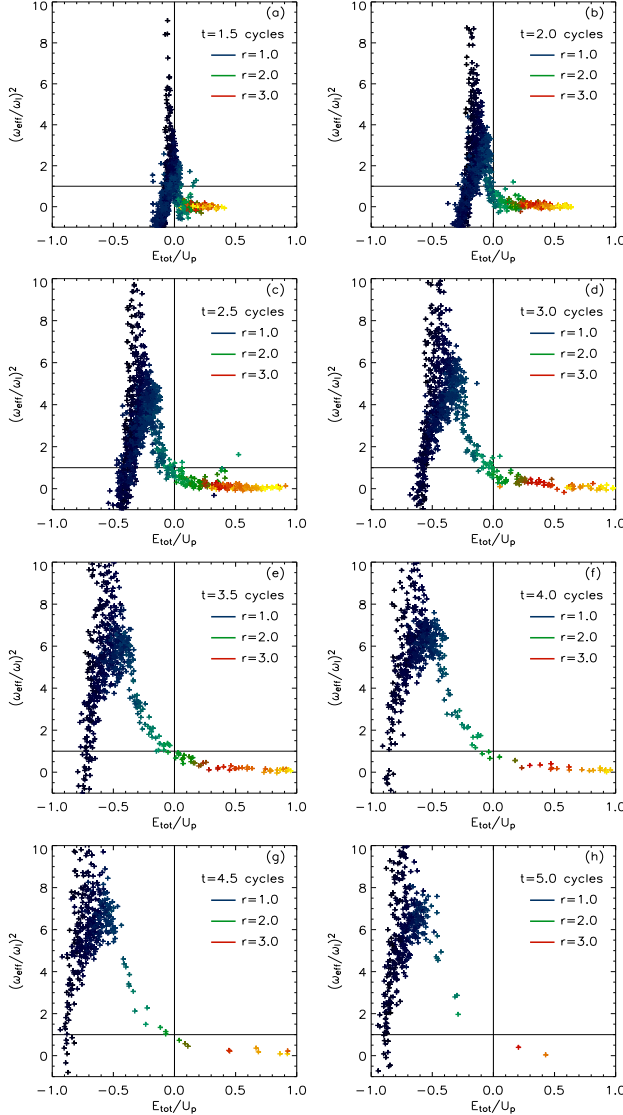


FIG. 12: (color online). Snapshots of PIC electrons in the frequency vs energy-plane for CP at times (a)  $t = 1.5$ , (b)  $t = 2.0$ , (c)  $t = 2.5$ , (d)  $t = 3.0$ , (e)  $t = 3.5$ , (f)  $t = 4.0$ , (g)  $t = 4.5$ , and (h)  $t = 5.0$  laser cycles for a laser intensity  $2.5 \times 10^{16} \text{ W cm}^{-2}$  and  $(\omega_{\text{Mie}}/\omega_l)^2 = 40/3$ . Other parameters as in Fig. 6. The radial positions (in units of  $R$ ) are color-coded. Electrons become free upon crossing the NLR, i.e.,  $(\omega_{\text{eff}}^2/\omega_l^2, E_{\text{tot}}/U_p) = (1, 0)$ .

ble mechanism behind outer ionization accompanied by efficient absorption of laser energy.

Finally, Fig. 13 shows the average value of the total absorbed energy per electron vs the peak laser intensity for cluster charge densities between  $\rho/\rho_c = 3-40$  in CP and LP laser fields. PIC results are compared with the RSM absorption results. The absorbed energy per electron in Figs. 13a-d is plotted in units of  $R^2\omega_l^2$  whereas the same results are shown in Figs. 13e-h in units of the ponderomotive energy  $U_p$ . The PIC results in Figs. 13a-d show that the absorbed energy increases linearly in the

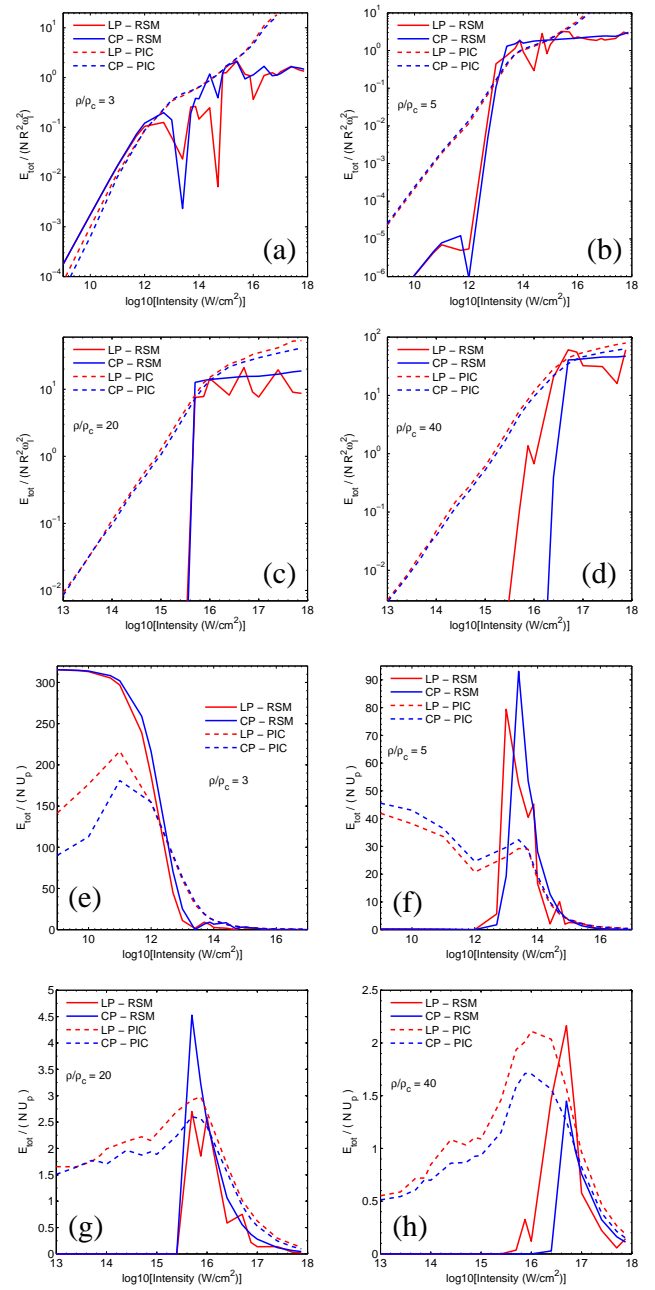


FIG. 13: (color online). Total absorbed energy per electron in units of  $R^2\omega_l^2$  vs laser intensity for charge densities (a)  $\rho/\rho_c = 3$  (linear resonance), (b)  $\rho/\rho_c = 5$ , (c)  $\rho/\rho_c = 20$ , and (d)  $\rho/\rho_c = 40$ . The absorbed energies for LP (red, lighter gray) and CP (blue, darker gray) using PIC (dashed) and the RSM (solid) are shown.

log-log representation up to a certain intensity and then tends to saturate due to the saturation of outer ionization. One sees that the saturation in the PIC results occur close to the RSM threshold intensity. Since with increasing charge density the restoring force due to the ions increases, the saturation of energy absorption in the RSM and PIC occur at higher laser intensities as the den-

sity increases from  $\rho/\rho_c = 3$  to  $\rho/\rho_c = 40$  in Fig. 13a–d. When outer ionization and the energy absorption saturate with increasing peak laser intensity, the average absorbed energy per electron divided by  $U_p$  (which is proportional to the so-called fractional absorption) starts decreasing in Figs. 13e–f. Figures 13a,e show that at linear resonance  $\rho/\rho_c = 3$ , the absorbed energy is already high at low values of the laser intensity ( $< 10^{12} \text{ Wcm}^{-2}$ ), and absorption is very efficient as compared to higher charge densities  $\rho/\rho_c = 5$ –40, presented in Figs. 13b–d and Figs. 13f–h. In fact, Fig. 13e illustrates that the absorbed energy is on the order of  $\sim 100U_p$  (both in the RSM and in the PIC) before the saturation of outer ionization. However, one should bear in mind that at too low laser intensities inner ionization would not occur in the first place so that in reality there would be no absorption at all.

Energy absorption in CP and LP laser fields at all intensities and all charge densities are almost equally efficient. Recalling that with our definition of the CP laser field the ponderomotive potential is equal for LP and CP while the electric field amplitude is not, we conclude that for the absorbed energy  $U_p$  matters while the NLR threshold is determined by the field strength.

The discrepancy between the PIC and RSM results at lower intensities is, again, due to the fact that the RSM provides a very well defined potential, although a more and more shallow one as the density decreases, in which the rigid electron sphere moves. In PIC, the potential is initially zero and builds up in the course of outer ionization. At higher intensities, the potentials for the remaining PIC electrons are closer to the RSM potential (see Fig. 7), explaining the improving agreement between RSM and PIC results as the laser intensity increases.

#### IV. SUMMARY

In summary, two different approaches to study collisionless laser energy absorption by clusters, namely (i) the rigid sphere model and (ii) particle-in-cell simulations, were pursued in this work. The goal was to identify the dominant mechanism of energy absorption and outer ionization of the cluster electrons in near infrared,

short laser pulses where collisional absorption is known to be inefficient. We showed that the cluster electrons contributing to efficient absorption and outer ionization undergo nonlinear resonance, meaning that the instantaneous frequency of their motion in a time-dependent, anharmonic, effective potential transiently meets the laser frequency. Nonlinear resonance is the only possible absorption mechanism if the laser pulse is too short for the linear resonance to occur (or during the early cluster dynamics in longer pulses) and if electron-ion collisions (inverse bremsstrahlung) are negligible. In order to prove the occurrence of nonlinear resonance we used a method to analyze the results obtained from particle-in-cell simulations, namely the mapping of the system of electrons and ions that interact through their mean field onto a system of nonlinear oscillators.

The occurrence of nonlinear resonance in the particle-in-cell simulations presented in this paper resembles the nonlinear resonance in the rigid sphere model. For a given cluster charge density, there is a threshold intensity around which the average electron energy displays a maximum conversion of laser energy. The threshold intensity can be calculated using the newly introduced vanishing barrier approximation. The common over-barrier approximation—applicable to atoms—fails in the case of finite-size potentials and underestimates the required laser field strength for ionization. This fact might be related to the experimentally observed “enhanced saturation intensity” in the ionization of finite-size systems such as  $C_{60}$ .

The efficiency of energy absorption from the laser is almost the same for linear and circular polarization, indicating that “collisions with the cluster boundary” as an explanation are misleading. Instead, nonlinear resonance is the main absorption mechanism in both cases. To illustrate this, the rigid sphere model has been extended for the circularly polarized laser pulses in this paper.

Future work will take self-consistent charge state distributions and mobile ions into account. Preliminary results indicate that nonlinear resonance clearly persists under these circumstances as well.

This work was supported by the Deutsche Forschungsgemeinschaft.

---

- [1] T. Ditmire, R.A. Smith, J.W.G. Tisch, and M.H.R. Hutchinson, Phys. Rev. Lett. **78**, 3121 (1997).
- [2] Molecules and clusters in intense laser fields, edited by Jan Posthumus (Cambridge University Press, Cambridge, U.K., 2001).
- [3] U. Saalmann and J.M. Rost, J. Phys. B: At. Mol. Opt. Phys. **39**, R39-R77 (2006).
- [4] V.P. Krainov and M.B. Smirnov, Phys. Rep. **370**, 237 (2002).
- [5] C. Rose-Petrucci, K.J. Schafer, K.R. Wilson, and C.P.J. Barty, Phys. Rev. A **55**, 1182 (1997).
- [6] D. Bauer and A. Macchi, Phys. Rev. A **68**, 033201 (2003).
- [7] T. Ditmire, J.W.G. Tisch, E. Springate, M.B. Mason, N. Hay, J. Marangos, and M.H.R. Hutchinson, Nature (London) **386**, 54 (1997).
- [8] V. Kumarappan, M. Krishnamurthy, and D. Mathur, Phys. Rev. A **67**, 043204 (2003).
- [9] E. Springate, S.A. Aseyev, S. Zamith, and M.J.J. Vrakking, Phys. Rev. A **68**, 053201 (2003).
- [10] K. Ishikawa and T. Blenski, Phys. Rev. A **62**, 063204 (2000).
- [11] F. Megi, M. Belkacem, M.A. Bouchene, E. Suraud, and

G. Zwicknagel, J. Phys. B: At. Mol. Opt. Phys. **36**, 273 (2003).

[12] C. Jungreuthmayer, M. Geissler, J. Zanghellini, and T. Brabec, Phys. Rev. Lett. **92**, 133401 (2004).

[13] D. Bauer, J. Phys. B: At. Mol. Opt. Phys. **37**, 3085 (2004).

[14] C. Siedschlag and J.M. Rost, Phys. Rev. Lett. **93**, 043402 (2004).

[15] C. Jungreuthmayer, L. Ramunno, J. Zanghellini and T. Brabec, J. Phys. B: At. Mol. Opt. Phys. **38**, 3029, (2005).

[16] T. Ditmire, T. Donnelly, A.M. Rubenchik, R.W. Falcone, and M.D. Perry, Phys. Rev. A **53**, 3379 (1996).

[17] T. Döppner, Th. Fennel, Th. Diederich, J. Tiggesbäumker, and K.H. Meiwes-Broer, Phys. Rev. Lett. **94**, 013401 (2005).

[18] L. Köller, M. Schumacher, J. Köhn, S. Teuber, J. Tiggesbäumker, and K.H. Meiwes-Broer, Phys. Rev. Lett. **82**, 3783 (1999).

[19] S. Zamith, T. Martchenko, Y. Ni, S.A. Aseyev, H.G. Muller, and M.J.J. Vrakking, Phys. Rev. A **70**, 011201(R) (2004).

[20] I. Last and J. Jortner, Phys. Rev. A **60**, 2215 (1999).

[21] Ulf Saalmann and Jan-Michael Rost, Phys. Rev. Lett. **91**, 223401 (2003).

[22] Th. Fennel, G.F. Bertsch, and K.H. Meiwes-Broer, Eur. Phys. J. D **29**, 367 (2004).

[23] C. Siedschlag and J.M. Rost, Phys. Rev. A **71**, 031401 (2005).

[24] T. Martchenko, Ch. Siedschlag, S. Zamith, H. G. Muller, and M. J. J. Vrakking, Phys. Rev. A **72**, 053202 (2005).

[25] M. Kundu and D. Bauer, Phys. Rev. Lett. **96**, 123401 (2006).

[26] T. Taguchi, T.M. Antonsen, Jr., and H.M. Milchberg, Phys. Rev. Lett. **92**, 205003 (2004); Thomas M. Antonsen, Jr. Toshihiro Taguchi, Ayush Gupta, John Palastro, and Howard M. Milchberg, Phys. Plasmas **12**, 056703 (2005).

[27] P. Mulser and M. Kanapathipillai, Phys. Rev. A **71**, 063201 (2005); P. Mulser, M. Kanapathipillai, and D.H.H. Hoffmann, Phys. Rev. Lett. **95**, 103401 (2005).

[28] D. Bauer and P. Mulser, J. Phys.: Conf. Ser. **11**, 169 (2005).

[29] Ph.A. Korneev, S.V. Popruzhenko, D.F. Zaretsky, W. Becker, Laser Phys. Lett. **2**, 452 (2005).

[30] P.B. Parks, T.E. Cowan, R.B. Stephens, and E.M. Campbell, Phys. Rev. A **63**, 063203 (2001).

[31] S.V. Fomichev, S.V. Popruzhenko, D.F. Zaretsky, and W. Becker, J. Phys. B: At. Mol. Opt. Phys. **36**, 3817 (2003).

[32] J.Y. Lin, H. Chu, M. Shen, Y. Xiao, C.H. Lee, S. Chen, and J. Wang, Optics Communications **231**, 375 (2004)

[33] V. Kumarappan, M. Krishnamurthy, D. Mathur, and L.C. Tribedi Phys. Rev. A **63**, 023203 (2001).

[34] S. Ter-Avetisyan, M. Schnürer, H. Stiel, U. Vogt, W. Radloff, W. Karpov, W. Sandner, and P.V. Nickles, Phys. Rev. E **64**, 036404, (2001).

[35] M. Krishnamurthy, D. Mathur, and V. Kumarappan, Phys. Rev. A **69**, 033202 (2004).

[36] C.K. Birdsall and A.B. Langdon, *Plasma Physics via Computer Simulation* (IOP, Bristol, 1991).

[37] G.L. Kotkin and V.G. Serbo, *Collection of problems in classical mechanics* (Pergamon, Oxford, 1971).

[38] H.A. Bethe and E.E. Salpeter, *Quantum mechanics of one- and two-electron atoms* (Plenum Publishing Corporation, New York, 1977).

[39] I.V. Hertel, T. Laarmann, and C.P. Schulz, Adv. At. Mol. Opt. Phys. **50**, 219 (2005).

[40] A. Jaron-Becker, A. Becker, and F.H.M. Faisal, Phys. Rev. Lett. **96**, 143006 (2006).